Anti-Corrosive, Microstructural and Physical Investigation of Zn-Cao Coated Steel

A. O. Derek[1], O. S. I. Fayomi[1, 2] and J. O. Atiba[1*]

[1]*Department of Mechanical Engineering, Bells University of Technology, Ota, Ogun State, Nigeria*
[2]*Department of Mechanical Engineering Science, University of Johannesburg, Johannesburg, South Africa*
Corresponding author: atibajoshua7@gmail.com

Received 26/04/2024; accepted 30/10/2024
https://doi.org/10.4152/pea.2026440403

Abstract
This study involved the development of a multifaceted Zn barrier coating through ED technique, followed by a comprehensive characterization of its properties. A MS plate, Zn and CaO were all sourced and assessed, in accordance with ASTM standards. ED process was then employed to coat MS, resulting in Zn-12CaO identification as the formulation with the highest coating thickness, at 0.2304 mm. Electrochemical assessment highlighted exceptional corrosion performance of Zn-12CaO coating, which showed CR of 2.4117 mm/year and P_r of 34.41 Ω. This performance stood out in comparison to the as-received sample, which had a CR of 13.449 mm/year across all Zn-CaO formulations. Microstructural analysis through SEM images unveiled the presence of rough and irregularly shaped refined particles, with the Zn-12CaO coating showing a significant deposit of crystallites. Furthermore, it exhibited remarkable hardness, registering a value of 258.12 BHN. EDS analysis provided insights into the coating's significant elements, contributing to its corrosion resistance and hardness properties. With its impressive hardness value of 258.12 BHN and low CR of 2.0618 mm/year, Zn-12CaO coating emerges as an excellent solution against potential failure in steel, for application in industries requiring durable protective barriers, such as automotive, construction and marine environments.

Keywords: corrosion; ED of Zn; mechanical properties; microstructural analysis.

Introduction•

MS is known to be a desirable material on local and industrial scales, owing to its unique properties that suit different applications [1, 2]. However, the metal has been known for its susceptibility to wear and corrosion after long repetitive use [3, 4]. Several techniques have been studied and utilized to protect steel and one common method used is ED, which is referred to as a method for developing or modifying new or existing materials via coatings or thin films approach [5]. ED process is

•The abbreviations list is in page 299.

associated with electroactive reduction or deposition, which is followed by a new species on the cathode surface [6]. ED significance lies in its controllability, which makes it applicable across diverse domains. Notably, ED has gained traction in coating applications, contributing to the field's advancement [7].

Over the past decades, coating industries have undergone increased technology and structural modifications. These changes occurred because of restrictions on the use of toxic and hazardous chemicals, which has led to the removal of previously well-established coatings by newer ones [8].

Zn has garnered significant attention in research as an ED material for safeguarding various steel types against corrosion and wear, due to its cost-effectiveness [9, 10]. However, despite its advantages, Zn still presents limitations in providing comprehensive corrosion protection to steel. Recent studies have indicated that alloying Zn with other metals during the coating process can lessen MS degradation [11]. Recognizing this gap in ED by Zn, the present study aims to investigate the impact of incorporating CaO, assessing microstructural, anti-corrosive and physical characteristics of the resulting composite material.

Materials and methods

MS and its depositing materials

MS, with the composition shown in Table 1, was purchased at an iron market in Ogun state. An elemental analysis revealed C and Fe levels of 0.216 and 98.1%, respectively. The main deposition element, Zn and the supplementary deposit, CaO, were sourced in Ogun state, Nigeria. Further elemental constituent analysis confirmed Zn bar chemical purity, which was 99.5%.

Table 1: Elemental constituent of the MS (SAE 1022) used.

Element	**C**	**Si**	**Mn**	**P**	**S**	**Ni**	**Cr**	**Cu**	**Fe**
Composition (wt.%)	0.216	0.161	0.613	0.018	0.027	0.009	0.031	0.006	Bal.

Substrate preparation

MS substrates were cut into five sections, each measuring 60 x 30 x 2 mm in size. These parts were subsequently employed as cathode electrode throughout the experiments. Acetone was used to thoroughly cleanse MS surface during the initial preparation, effectively removing any rust or impurities. To improve the MS surface quality even further, emery paper of various grades was used to polish it, removing any existing rust, similarly to procedures carried out by [12]. The anode in the electroplating process was a Zn bar that was activated with a diluted HCl solution.

Coating bath and its ED process

The coating bath used in this study was made up of sulphate salts, principally consisting of soluble sulphate compounds with different individual molar

concentrations. This bath acted as an electrolyte during the ED process, allowing the contemporaneous deposition of metallic components to produce coatings with improved alloy compositions. The surface morphology of these coatings was further herein investigated. The method began with the addition of 1000 mg distilled water to a beaker. As shown in Table 2, the bath's composition included a variety of salts and CaO as primary inorganic oxide. Each constituent had a consistent mass content (g/L).

Table 2: Bath composition of the deposition.

Chemical composition	CaO	Boric acid	Thiourea	Na_2SO_4	K_2SO_4	$ZnSO_4$	$(NH_4)_2SO_4$
Mass (g/L)	0-12	10	10	10	15	15	5

During ED procedure, MS samples complied with ASTM A53M standards. Before coating, the polished MS surfaces were cleaned in 0.01 M Na_2CO_3, for 10 sec. and briefly immersed in 10% HCl, at room temperature. The coating procedure began with transferring the prepared bath to a beaker, then heating it to 47 °C and keeping it at that temperature. Cu wire anodes were placed into the bath 50 mm apart, while a one of them was linked to MS samples (cathode) and immersed within the bath. MS sample was put such as to ensure equal spacing between Zn bars. A 200 rpm swirling mechanism within the bath avoided particle agglomeration, while boosting electrophoresis, to assist ion transport towards the cathode (steel). The deposition lasted 20 min at a voltage of 4.8 V and J_{corr} of 1 A/cm^2. Following preliminary testing, process parameters were developed (Table 3). Following deposition, the coatings were air-dried and kept in an oxygen-free media. These coated samples were then dimensioned down to 10 x 10 x 2 mm, for additional testing and characterization, with the resulting samples being coded as Zn-3CaO, Zn-6CaO, Zn-9CaO and Zn-12CaO.

Table 3: Process parameters of deposition.

Parameters	Values
pH	4.8
Cell voltage	3.2 V
J_{corr}	1 A/cm^2
Time	20 min
Stirring rate	200 rpm
Temperature	47^{o}C

Electrochemical analysis

PDP tests were used in this work to analyze the samples' corrosion behavior. Within a three-electrode cell configuration, a non-aqueous Ag/Ag terminal served as reference electrode, while an Al wire was the counter electrode. The steel coated sample was securely positioned as working electrode. Several electrochemical

characteristics were evaluated, including J_{corr}, E_{corr}, P_r and CR. Eq. (1) was used to calculate corrosion IE(%). The samples were manually treated with 1,200 grit emery paper before being cleaned with double-distilled water in preparation for the electrochemical experiments. Then, the samples were placed in the test solution-containing cell. Before polarization curves, a 120 sec. immersion ensured a stable OCP. The voltage was changed from -1.5 to +1.5 V, at a scan rate of 0.1 mV/s. Electrochemical tests were carried out with the help of a Potentiostat/Galvanostat apparatus, which was operated by NOVA software version 2.1.2. The test media was a 1 M HCl solution.

$$\% \text{ IE} = \frac{i0corr - icorr}{i0cor} \times 100 \quad (1)$$

where i^0_{corr} and i_{corr} J_{corr} without and with inhibitor, respectively.

Physical characterization

A small thickness gauge with an accuracy of ±0.05 was used to measure coating thickness. This evaluation was carried out at three independent sites on the samples, and the resulting average thickness was determined. BHN test was carried out on a hardness machine able to support loads from 2.5 to 187.5 kgf. The samples were subjected to a 30 kgf force (P), for 30 sec, using a hardened indenting steel ball with a diameter of 10 mm. Using a small microscope, measurements of the indentation diameter were taken and documented. Following that, BHN values for the materials were computed using Eq. (2).

$$\text{BHN} = \frac{2P}{\pi D\,[D - \sqrt{(D^2 - d^2)}]} \quad (2)$$

Microstructural evaluation

XRD/EDS were deployed to characterize the developed samples surfaces for determining their morphologies. EDS was used to determine the elements present in the developed barrier coating. XRD analysis utilized a Rigaku D/Max-llC X-ray diffractometer, equipped with CuKa radiation operating at 40kV and 20mA. Scanning process involved capturing diffractions at a rate of 0/min within the range of 2 to 500, all conducted at room temperature. Collected diffraction data were compared with standard mineral data present in ICDD mineral powder diffraction file, encompassing information on a broad spectrum of over 3000 minerals. Notably, diffraction data for coated samples were found to align with those of standard minerals.

Results and discussion

Mass gained and coating thickness of coated samples

Table 4 presents the alterations in mass before to and after the coating process, alongside with cumulative mass gain after coating. The findings unveiled that Zn-12CaO coated sample underwent the most substantial mass augmentation, totaling

approximately 0.31 g. This outcome suggests a heightened particle adherence to the substrate during the coating procedure. Similarly, Fig. 1 graphically illustrates the samples' coating thickness, determined by a specialized coating thickness gauge device. Notably, Zn-12CaO exhibited the most noteworthy coating thickness of 0.2304 mm. The enhancement in coating thickness was influenced by pivotal factors such as substrate thickness, the steel surface state and its chemical composition [13, 14].

Table 4: Coating mass gaining for the first phase ED.

Sample	Mass before coating (g)	Mass after coating (g)	Mass gained (g)
As-received	9.54	0	0.00
Zn-3CaO	9.52	9.72	0.20
Zn-6CaO	9.58	9.79	0.21
Zn-9CaO	9.61	9.83	0.22
Zn-12CaO	9.57	9.88	0.31

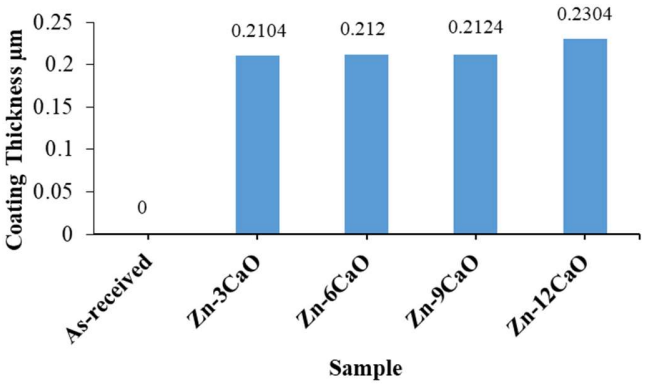

Figure 1: Coating thickness for the first ED phase of deposition.

Electrochemical analysis of Zn-CaO coated samples

Table 5 and Fig. 2 showcase polarisation data and associated curve for Zn-CaO ED. The as-received sample displayed the highest CR (13.449 mm/year) and J_{corr}, along with a lower Pr (8.17 Ω), compared to coated samples, with higher resistance. This aligns with the study by [15], indicating poorer corrosion resistance for as-received samples. Zn-3CaO exhibited reduced CR and J_{corr}, yet a higher P_r (11.61 Ω) compared to as-received, signifying improved resistance to chloride penetration. Zn-6CaO showcased a lower CR (4.9702 mm/year) and notable P_r (13.82 Ω), indicating remarkable corrosion reduction compared to both as-received and Zn-3CaO conditions. Furthermore, Zn-9CaO and Zn-12CaO displayed reduced CR of 2.6563 and 2.4117 mm/year, respectively, in comparison to both as-received and previously discussed coated samples. This heightened corrosion resistance is due to the smaller crystallite size of Zn-CaO. Particularly, Zn-12CaO exhibited the highest corrosion resistance among the samples, accompanied by the highest polarization value of 34.41 Ω, resulting in reduced J_{corr} (Table 5). Increasing CaO content aided in the formation of a refined structure that acted as a protective film within Zn-CaO mix, subsequently

elevating corrosion resistance [16]. Further analysis of Table 5 and Fig. 2 demonstrates that the coated samples exhibit enhanced cathodic protection compared to as-received ones, which is evident in negative E_{corr} values variance [17].

Table 5: Polarization data for Zn-CaO coated samples.

Sample	E_{corr} (V)	J_{corr} (A/cm^2)	Cr (mm/year)	Pr (Ω)	βa (V/dec)	βc (V/dec)
As-received	-1.0957	1.157E-03	13.449	8.17	0.0341	0.0603
Zn-3CaO	-0.7112	5.199E-04	6.042	11.61	0.0082	0.0172
Zn-6CaO	-1.0647	4.277E-04	4..9702	13.82	0.0218	0.0098
Zn-9CaO	-1.0677	2.286E-04	2.6563	22.11	0.0216	0.0741
Zn-12CaO	-1.0672	2.076E-04	2.4117	34.41	0.0849	0.0564

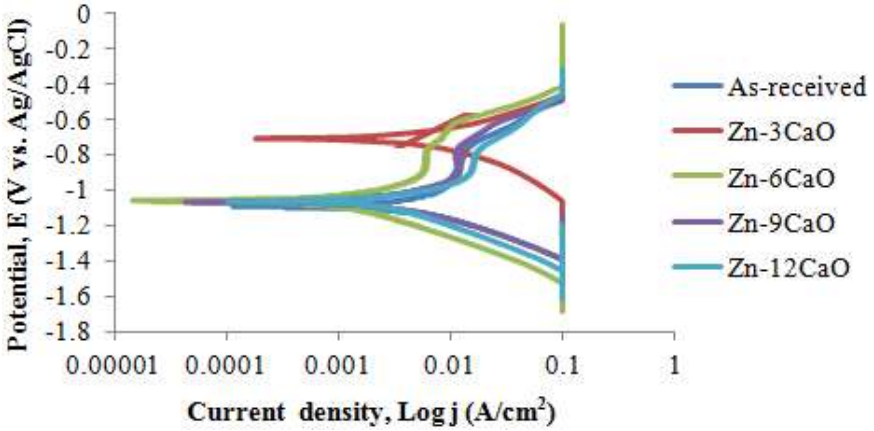

Figure 2: Polarization curves for Zn-CaO coated samples.

Fig. 3 displays OCP evolution across various coatings.

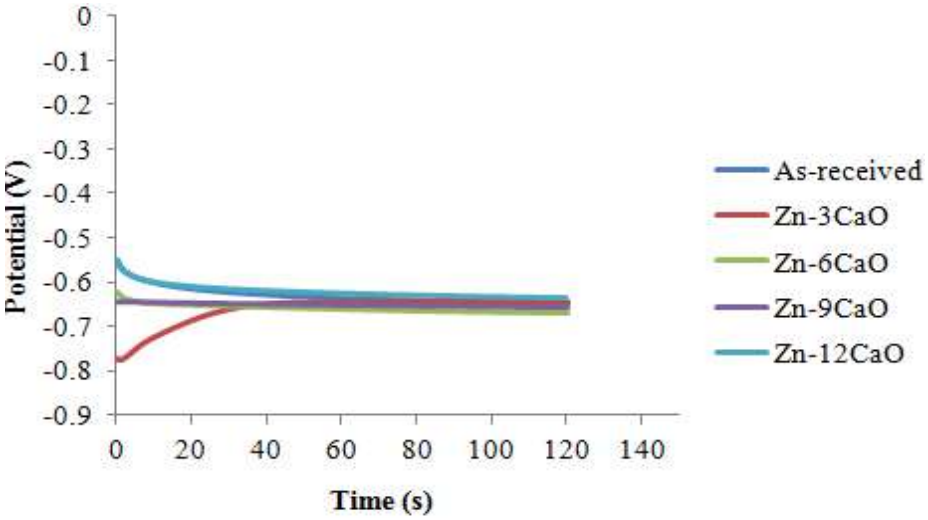

Figure 3: OCP for Zn-CaO coated samples.

The uncoated sample showed an initial shift towards negative direction within the first 18 sec., followed by stabilization until the end of the test period (120 sec). Similarly, the coated samples exhibited an initial increase towards more negative values for approx. 30 sec., followed by stability for the subsequent one-hundred and twenty 120) sec. This behaviour was due to CaO films dissolution caused by the aggressive environment. The change in OCP indicated that CaO molecules mitigated the environment's aggressiveness, by shifting potentials towards more negative values [18], with the exception of the Zn-9CaO sample, which remained constant.

Microstructural properties of Zn-CaO coated samples

Fig. 4 depicts SEM/EDS morphology of the as-received steel sample prior to ED. Upon examining SEM image, it becomes evident that the surface was exceptionally smooth and well-polished.

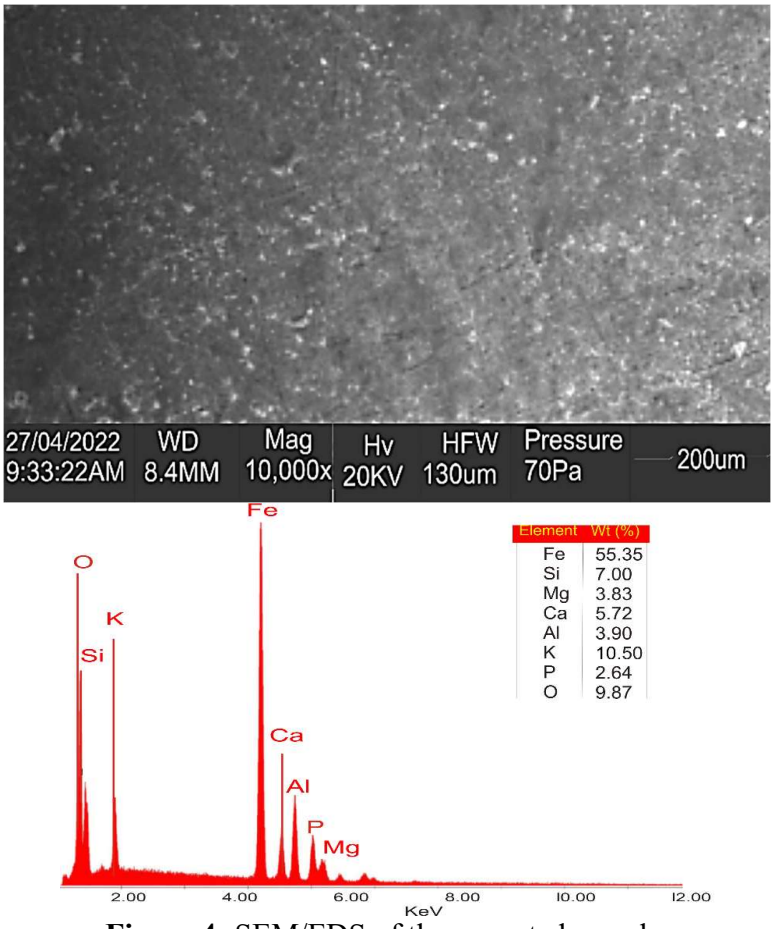

Figure 4: SEM/EDS of the uncoated sample.

Fig. 5 presents SEM and EDS analyses of Zn-CaO coated samples. The results unveil distinct and uniformly distributed morphologies in the microstructure. Within

the SEM image, rough and irregular refined particles are seen. Furthermore, SEM image reveals varying particle sizes, indicating their reduced dimensions and expanded pore sizes. This characteristic contributes to the coating enhanced corrosion resistance. Notably, some regions within the SEM image display a cake-like structure, while other areas showcase a reorganized pattern of particle aggregation. These traits align with findings reported by [19, 20]. Importantly, these features correlate with variations in electrochemical potential disparities across the coated sample's surface.

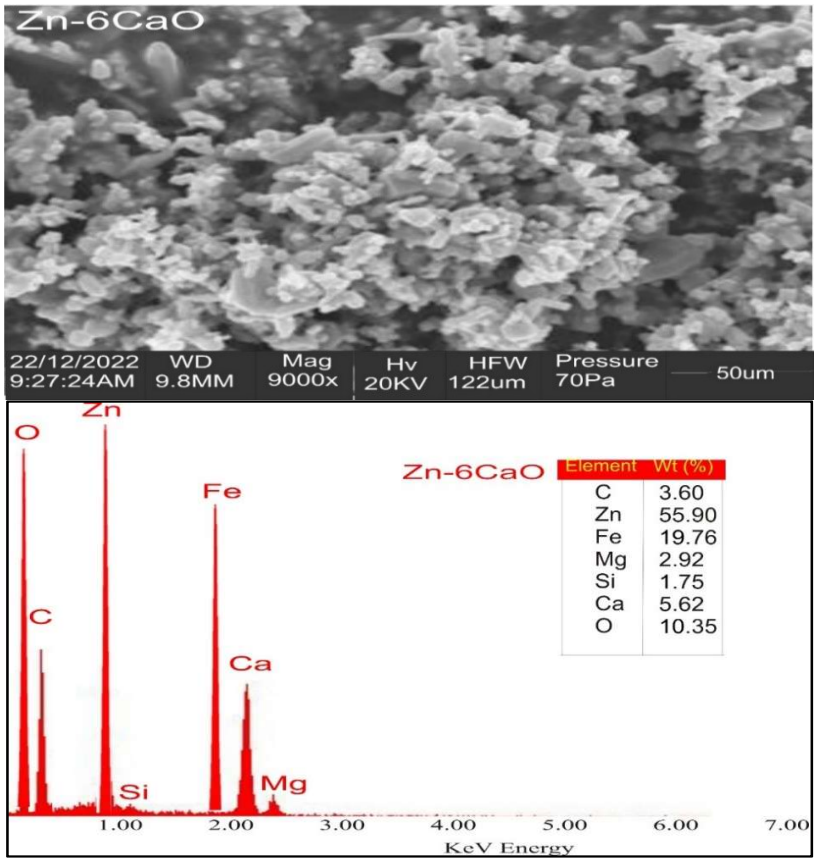

Figure 5: SEM/EDS of Zn-6CaO.

EDS analysis of Zn-CaO coated samples unveiled significant elements such as C, Zn, Fe, Mn, Si, Ca and O, with weight percentages of 3.60, 55.90, 19.76, 2.92, 1.75, 5.62 and 10.35, respectively. The presence of Ca in the coating is due to deposited CaO. Notably, higher levels of Zn and O were present in the coating. Zn is renowned for its rapid activation speed and ample surface area, offering enhanced cathodic protection in defects regions on the parent metal. This abundant Zn and O content likely arises from ZnO deposition. Fig. 6 illustrates XRD profile of Zn-CaO coating. The plot indicates prominent peaks at 2θ=25° for Zn (Ca), and 2θ=35° for

Fe, suggesting their prevalence in the coating's morphology. The robust presence of Zn/Ca at a major peak indicates full crystallinity within the coating's structure, contributing to reduced J_{corr} [21]. XRD plot unveils various Zn phases, with Zn/Ca being the most dominant, which reveals preferable growth conditions for Zn crystals. Similarly, higher diffraction peaks appear for Fe/Zn/Ca) and Fe/Zn/Ca/Si, at 2θ=15° and 2θ=22°, respectively. Lower diffraction peaks were seen for Mg/Zn, at 2θ=28°, and for Fe/Ca) and Fe/Mn, at 2θ=48° and 2θ=58°, respectively. These XRD patterns collectively elucidated the coating crystalline structure, revealing detailed elemental and compound information from EDS study.

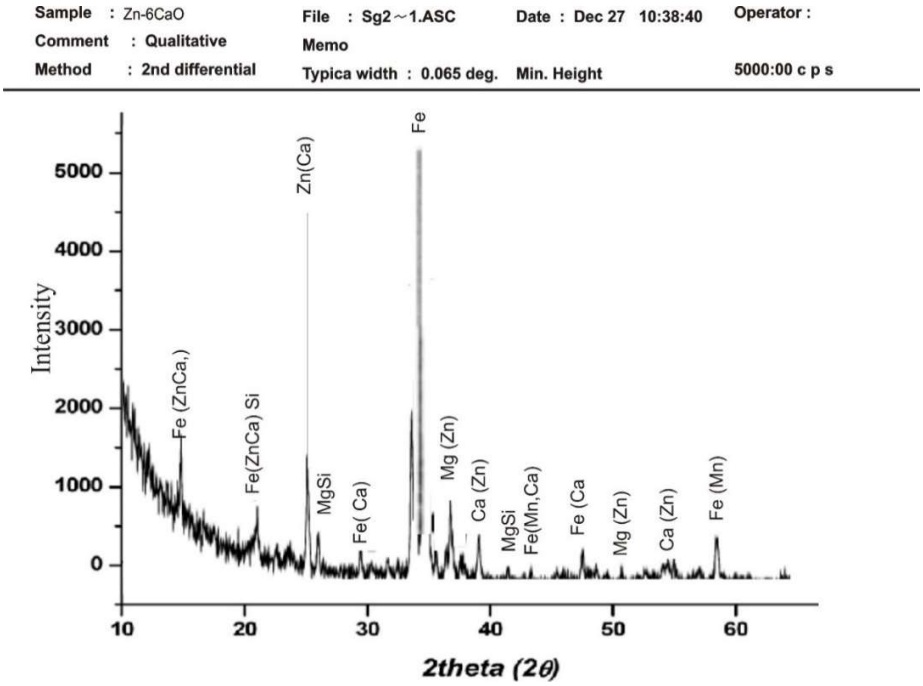

Figure 6: XRD Profile of Zn-6CaO.

Brinell hardness of the Zn-CaO coated samples

Fig. 7 illustrates the diverse hardness values of Zn-CaO coated samples. The results reveal a noticeable enhancement in hardness properties of the coated samples compared to as-received ones. This improvement in hardness properties demonstrates a consistent trend corresponding to the composition of the coated samples, ranging from 3 to 12%. The specific hardness values are as follows: 242.72 BHN for Zn-3CaO exhibits; 252.28 BHN for Zn-6CaO; 253.56 BHN for Zn-9CaO; and 258.18 BHN for Zn-12CaO. In contrast, the as-received sample's hardness values were 137.12 BHN. This progression in hardness aligns with the weight composition trend, as previously indicated by [22]. Remarkably, Zn-12CaO boasts the highest hardness value of 258.12 BHN, signifying an impressive 88.24%

increase relative to the as-received state. This exceptional hardness enhancement was due to the refined structure present within the coated sample.

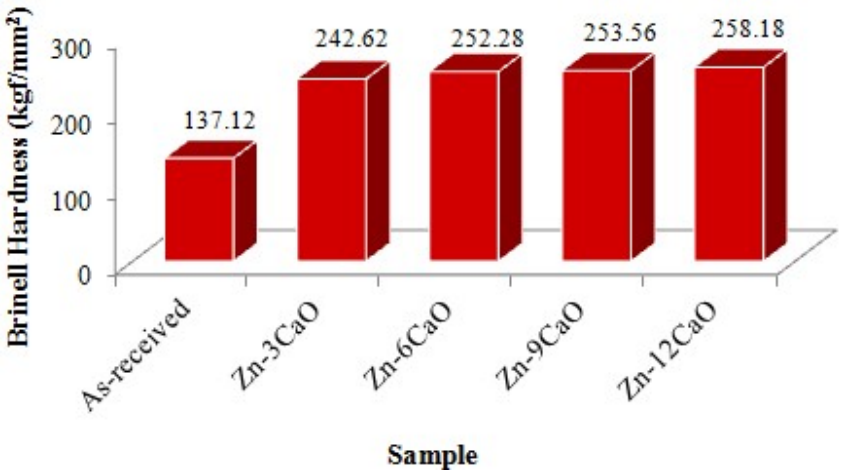

Figure 7: BHN of Zn-CaO coated samples.

Conclusion

Zn-12CaO coating thickness was the greatest, measuring 0.2304 mm. This increase in thickness can be due to the additives, which promoted the formation of grain boundaries within the coating, s improving its overall qualities. Furthermore, the observed increase in coating thickness corresponded to a proportional drop in cathodic J_{corr}. Coated materials exhibited excellent corrosion resistance when compared to as-received materials, with Zn-12CaO having a CR of 2.4117 mm/yr.

A substantial enhancement in hardness was evident in the coated samples compared to the uncoated one, which possessed a hardness of 137.12 BHN. Across all Zn-CaO coatings, impressive hardness levels were achieved in relation to the as-received sample, with the peak value reaching 258.18 BHN.

Notable enhancements were observed in the coating's surface morphology, confirmed by significant elemental composition in EDS results and microstructural homogeneity indicated by XRD profile.

Acknowledgements

The support of Bells university of Technology is deeply appreciated.

Conflict of interest

The researchers declare that there is no conflict of interest during and after the study.

Authors' contributions

A. O. Derek: experimentation. **O. S. I. Fayomi**: project supervision. **J. O. Atiba**: manuscript writing.

Abbreviations

ASTM: American Society for Testing and Material
BHN: Brinell hardness number
CaO: calcium oxide
CR: corrosion rate
E_{corr}: corrosion potential
ED: electrodeposition
EDS: energy-dispersive X-ray spectroscopy
J_{corr}: corrosion density
MS: mild steel
OCP: open circuit potential
P_r: polarization resistance
Rpm: rotation per minute
SEM: scanning electron microscopy
XRD: X-ray crystallography

References

1. Gedge G. Structural uses of stainless steel—buildings and civil engineering. J Constr steel Res. 2008;64(11):1194-8. https://doi.org/10.1016/j.jcsr.2008.05.006
2. Baddoo NR. Stainless steel in construction: A review of research, applications, challenges and opportunities. J Constr Steel Res. 2008;64(11):1199-206. https://doi.org/10.1016/j.jcsr.2008.07.011
3. Rahman Rashid RA, Javed MA et al. Effect of *in situ* tempering on the mechanical, microstructural and corrosion properties of 316L stainless steel laser-cladded coating on mild steel. Int J Adv Manuf Technol. 2021;117(9-10):2949-58. https://doi.org/10.1007/s00170-021-07886-7
4. Fayomi OSI, Akande G, Daramola D et al. Inhibitive Characteristics of Cefalexin Drug Addition on Corrosion Evolution of Mild Steel in a Chloride Medium. Port Elctrochim Acta. 2021;39(2):149-57. https://doi.org/10.4152/pea.202102149
5. Loukil N, Feki M. Zn–Mn electrodeposition: a literature review. J Electrochem Soc. 2020;167(2):22503. https://doi.org/10.1149/1945-7111/ab6160
6. Paul S, Maniam K,. Progress in Electrodeposition of Zinc and Zinc Nickel Alloys Using Ionic Liquids. Appl Sci. 2020;10(15):5321. https://doi.org/10.3390/app10155321
7. Islam S, Mia MM, Shah SS et al. Recent Advancements in Electrochemical Deposition of Metal-Based Electrode Materials for Electrochemical Supercapacitors. Chem Rec. 2022;22(7):e202200013. https://doi.org/10.1002/tcr.202200013

8. Bayer IS. Superhydrophobic coatings from ecofriendly materials and processes: a review. Adv Mater Interfaces. 2020;7(13):2000095. https://doi.org/10.1002/admi.202000095
9. Abioye OP, Musa AJ, Loto CA et al. Evaluation of Corrosive Behavior of Zinc Composite Coating on Mild Steel for Marine Applications. J Phys Conf Ser. 2019;1378(4): 042051. https://doi.org/10.1088/1742-6596/1378/4/042051
10. Kumar A, Sammaiah DP. Influence of process parameters on mechanical and metallurgical properties of zinc coating on mild steel during mechanical process. Curr Res Top poweer, Nucl Fuel Energy, SP-CRTPNFE. 2017.
11. Elewa RE, Fayomi OSI, Afolalu SA et al. Material selection and corrosion assessment of galvanized roofing sheet: Potentiodynamic investigation, mathematical modeling and simulation. Rasay J Chem. 2021;14(1):111-24. https://doi.org/10.31788/RJC.2021.1415921
12. Fayomi OSI, Akande IG, Popoola API et al. Structural characterization and corrosion properties of electroless processed NiPMnO2 composite coatings on SAE 1015 steel for advanced applications. J Sci Adv Mater Dev. 2019;4(2):285-9. https://doi.org/10.1016/j.jsamd.2019.04.001
13. Michal P, Gombár M, Vagaská A et al. Experimental study and modeling of the zinc coating thickness. Adv Mater Res. 2013;712:382-6. https://doi.org/10.4028/www.scientific.net/AMR.712-715.382
14. Basiaga M, Walke W, Kajzer W et al. Atomic layer deposited ZnO films on stainless steel for biomedical applications. Arch Civ Mech Eng. 2021;21:1-15. https://doi.org/10.1007/s43452-020-00148-5
15. Wang Y, Xiong X, Ju BF et al. Voxelated meniscus-confined electrodeposition of 3D metallic microstructures. Int J Mach Tools Manuf. 2022;174:103850. https://doi.org/10.1016/j.ijmachtools.2022.103850
16. Nam ND, Bian MZ, Forsyth M et al. Effect of calcium oxide on the corrosion behaviour of AZ91 magnesium alloy. Corros Sci. 2012;64:263-71. https://doi.org/10.1016/j.corsci.2012.07.026
17. Schmitt J, Schindler M, Oberbauer A et al. Determination of degradation modes of lithium-ion batteries considering aging-induced changes in the half-cell open-circuit potential curve of silicon–graphite. J Pow Sour. 2022;532:231296. https://doi.org/10.1016/j.jpowsour.2022.231296
18. Sherif ESM, Abbas AT, Gopi D et al. Corrosion and corrosion inhibition of high strength low alloy steel in 2.0 M sulfuric acid solutions by 3-amino-1, 2, 3-triazole as a corrosion inhibitor. J Chem. 2014:1-8. https://doi.org/10.1155/2014/538794
19. Aslam S, Bokhari TH, Anwar T et al. Graphene oxide coated graphene foam based chemical sensor. Mater Lett. 2019;235:66-70. https://doi.org/10.1016/j.matlet.2018.09.164

20. Fatoba OS, Popoola API, Aigbodion VS. Electrochemical studies and surface analyses of laser deposited Zn-Al-Sn coatings on AISI 1015 steel. Int J Surf Sci Eng. 2018;12(1):40-59. https://doi.org/10.1504/IJSURFSE.2018.090054
21. Vourlias G. Application of X-rays diffraction for identifying thin oxide surface layers on zinc coatings. Coatings. 2020;10(10):1005. https://doi.org/10.3390/coatings10101005
22. Fatoba OS, Popoola API, Aigbodion VS. Laser Alloying of an Al-Sn Binary Alloy onto Mild Steel: In Situ Formation, Hardness and Anti-corrosion Properties. Lasers Eng. 2018;39:292-312.